NJC

ROYAL SOCIETY OF CHEMISTRY

PAPER

Published on 12 November 2025
Licence and permissions

Check for updates

Cite this: *New J. Chem.*, 2025, **49**, 20272

A highly hydrophobic polyhedral oligomeric silsesquioxane platform intended for microplastic adsorption and oil remediation

Delaram-Sadat Tavoussi-Shirazi,[a] Nasrin Moradi,[a] Mehrdad Mohaghegh,[a] Majid Karimi[b] and Habib Bagheri *[a]

Received 19th August 2025,
Accepted 28th October 2025

DOI: 10.1039/d5nj03353e

rsc.li/njc

The ubiquity and persistence of microplastics (MPs) and hydrophobic organic pollutants pose serious threats to aquatic environments and human health, necessitating the development of effective remediation strategies. In this study, a fluorine-free polyhedral oligomeric silsesquioxane (POSS) functionalized platform was successfully fabricated *via* a UV-assisted thiol–ene click reaction without any initiator. The platform contained both SH- and OV-POSS, which led to a sponge with durable superhydrophobicity, enhanced stability, and dual adsorption capability toward oils and microplastics. The structural and chemical features of the POSS modified sorbent were systematically confirmed using scanning electron microscopy (SEM), Fourier-transform infrared spectroscopy (FTIR), energy-dispersive spectroscopy (EDS), and Brunauer–Emmett–Teller (BET) surface area analysis. The modified platform by POSS features a highly interconnected porous structure and enhanced surface hydrophobicity (water contact angle: 153°). Kinetic and isotherm analyses demonstrate that the adsorption process follows a pseudo-second-order kinetic model and is best described by the Freundlich isotherm, indicating multilayer adsorption on heterogeneous surfaces. The modified platform rapidly adsorbed nearly 90% of MPs from aqueous suspension, maintaining high removal efficiency even after multiple reuse cycles. The POSS modified sponge also shows outstanding oil and organic solvent sorption capacities and retains its efficiency after performing multiple absorption/desorption cycles, and an absorption capacity of up to 89 g g^{-1} for oil/organic solutions was achieved. Overall, the POSS-functionalized sponge proves to be a sustainable, efficient, and versatile platform for large-scale water treatment applications targeting both microplastics and oil pollution removal from aquatic media.

1. Introduction

Plastics have become ubiquitous in modern society due to their versatility and durability,[1] with global production surpassing 335 million tons annually. Despite this widespread use, only approximately 9% of plastic waste is effectively recycled, resulting in significant environmental accumulation. Microplastics (MPs), in particular, defined as plastic particles ranging from 1 μm to 5 mm,[2] arise primarily through the fragmentation of larger plastic debris *via* physical abrasion, chemical oxidation, ultraviolet (UV) radiation exposure, combustion, and biodegradation.[3,4] Over the past decade, MPs have garnered increasing attention from researchers and environmentalists owing to their pervasive presence and persistence in aquatic ecosystems worldwide.[5] Due to their tiny particle size, MPs are readily ingested by various aquatic organisms such as fish and bivalves, leading to bioaccumulation and potential transfer through the food web.[6] Moreover, MPs possess a high specific surface area and hydrophobic nature that facilitate adsorption of toxic pollutants and pathogenic microorganisms. These factors collectively pose risks to aquatic biota and human health, including immune dysfunction and localized inflammatory responses upon ingestion.[7,8] Consequently, the effective removal of MPs from aqueous environments is imperative to mitigate their ecological and health hazards. Simultaneously, oils and organic solvents are regarded as major aquatic pollutants, with their prevalence exacerbated by increasing industrial activities and expansion of waterborne transportation.[9] Therefore, remediation strategies addressing both MPs and oil pollutants are essential to restore water quality and safeguard environmental and public health.[10] Current techniques for the separation and removal of MPs and oil contaminants broadly include physical, chemical, and biological methods.[11]

[a] *Department of Chemistry, Sharif University of Technology, P.O. Box 11155-9516, Tehran, Iran. E-mail: bagheri@sharif.edu*
[b] *Polymerization Engineering Department, Iran Polymer and Petrochemical Institute (IPPI), P.O. Box 14965/115, Tehran, Iran*

Physical methods such as filtration and sedimentation often suffer from inefficiency in capturing particles at the micro scale. Chemical treatments can generate secondary pollutants, while biological approaches may require extended treatment times and controlled conditions. Wastewater treatment plants (WWTPs), despite serving as primary barriers to MPs' discharge, typically achieve only about 90% removal efficiency, with a substantial fraction of MPs below 25 μm escaping treatment.[12] Moreover, challenges such as membrane fouling, operational complexity, and high material costs hinder the widespread application of advanced removal technologies.[13] Adsorption has emerged as a promising approach for MPs and oil remediation due to its advantages including high removal efficiency, operational simplicity, low cost, fast kinetics, and minimal generation of toxic byproducts.[14] Diverse adsorbents such as metal–organic frameworks (MOFs),[15] layered double hydroxides (LDHs),[16] magnetic materials,[17] biochar,[18] zeolitic imidazolate frameworks (ZIFs),[19] and engineered sponges have demonstrated efficacy in capturing MPs from aqueous matrices.[20] Among these, sponge-based adsorbents present unique advantages attributable to their three-dimensional interconnected porous structures, high accessible pore volume, mechanical flexibility, and excellent reusability.[21] Their facile fabrication, broad applicability, and ease of operation position them as attractive candidates for practical water treatment solutions.[22] Notwithstanding these benefits, limitations such as suboptimal adsorption rates, environmental sensitivity (*e.g.*, to pH), and the need for enhanced selectivity remain challenges to be addressed.[15] Considering the hydrophobic nature of MPs, the application of hydrophobic adsorbents is essential for their efficient removal from aqueous environments. The hydrophobicity of a surface is primarily governed by the intentional engineering of its micro and nanoscale structures to create surface roughness, in conjunction with the application of low-surface-energy materials capable of inducing a Cassie–Baxter wetting state.[23] Hydrophobic modification of adsorbents is thus crucial for enhancing their MP removal capability, and numerous strategies have been developed for the fabrication of highly hydrophobic surfaces.[24] However, many conventional methods rely on toxic or environmentally unsustainable components such as fluorocarbons,[25] underscoring the importance of identifying and employing non-toxic alternatives. In this context, polyhedral oligomeric silsesquioxanes (POSSs) have emerged as ideal reagents for advanced material design. POSS is an organic–inorganic hybrid material at the molecular level, represented by the general formula $(RSiO_{3/2})_n$, featuring a rigid, three-dimensional silicon–oxygen cage structure (approximately 1–3 nm) decorated with organic functional groups. This unique architecture imparts POSS with outstanding chemical and thermal stability, non-toxicity, and high hydrophobicity, while its odorless and environmentally friendly nature, attributed to its non-toxic inner silica core, prevents the release of volatile organic byproducts during synthesis.[26–28] As a result, POSS represents a promising and sustainable alternative for the hydrophobic modification of adsorbents aimed at efficient MP removal and hydrophobic organic pollutant sorption. Zhang *et al.* developed UV-curable hydrophobic coatings based on epoxy-functionalized POSS (EP-POSS) and its derivatives. By incorporating alkyl and fluoroalkyl EP-POSSs with silica nanoparticles and photoinitiators, the resulting hybrid coatings showed high mechanical strength and sufficient hydrophobicity (WCA up to 108°).[29] Similarly, Hao *et al.* fabricated 3D polymer sponges functionalized with POSS-based organosilicon precursors, achieving a highly hydrophobic (WCA > 150°) property. The incorporation of POSS effectively reduced surface energy and improved mechanical strength.[30] Wanli *et al.* developed dual-fluorinated POSS hybrid polymers as durable superamphiphobic coatings on textiles and aluminum *via* dip-coating which showed anti-corrosive properties with contact angles above 160°.[31] Most previous POSS-based studies improved hydrophobicity using fluorinated agents such as perfluoro-POSS or long-chain fluorosilanes, which raise environmental concerns. Moreover, conventional dip- and spray-coating methods involve volatile solvents and poor surface uniformity.[32]

The aim of this study was to prepare an environmentally friendly medium capable of efficiently removing both MPs and oil contaminants from water. In this context, the development of next-generation, high-efficiency hydrophobic sponge-based sorbents capable of simultaneously removing microplastics and oil contaminants represents a significant advancement toward effective, sustainable water treatment technologies. This study reports the synthesis, characterization, and performance evaluation of a hydrophobic sponge designed for efficient sorption of MPs and hydrophobic organic pollutants from water. The sorption mechanisms, regeneration capability, and comparative performance with existing materials are systematically investigated, highlighting the material's potential for large-scale environmental remediation.

2. Experimental section

2.1. Chemicals

All chemicals were used as received without any further purification. Sodium chloride (NaCl), potassium chloride (KCl), and calcium chloride ($CaCl_2$) were purchased from Sigma-Aldrich (St. Louis, MO, USA). Carbon tetrachloride, ammonia, and sodium hydroxide (NaOH) were obtained from Merck (Darmstadt, Germany). Melamine sponges were procured from a local shop. Two types of polymer powders, polyvinyl chloride (PVC) and polystyrene (PS), were purchased and used as received. Organic solvents including acetone (99%), *n*-dodecane (99%), toluene (99%), *n*-hexane, dichloromethane (DCM), and ethanol were purchased from Merck (Darmstadt, Germany). Methanol (MeOH, HPLC grade) was obtained from Baher Exir Kaveh (Saveh, Iran). Sodium sulfate (Na_2SO_4) was also sourced from Merck (Darmstadt, Germany). Additional reagents included vinylmethoxysilane, hydrochloric acid (HCl, 36.5%), 3-(trimethoxysilyl)-1-propanethiol, and (3-mercaptopropyl)trimethoxysilane (MTS), all purchased from Sigma-Aldrich (St. Louis, MO, USA).

2.2 Apparatus

The morphology and surface structures of the sponges were examined by scanning electron microscopy (SEM) using a TESCAN Mira 3-XMU (Czech Republic). Samples were mounted on carbon tape and sputter-coated with gold prior to imaging. Surface functional groups were analyzed using Fourier-transform infrared spectroscopy (FTIR), including ATR-FTIR (AVATAR, Thermo, USA). The specific surface area and porosity were determined by nitrogen adsorption–desorption isotherms using the Brunauer–Emmett–Teller (BET) method on a BELSORP-mini II instrument (BEL Japan), with samples degassed at 70 °C for three hours prior to measurement. Zeta potential measurements of MPs and the sponge were conducted using a Zetasizer Nano ZS90 (Malvern Instruments, UK) across a range of initial pH values. An Elmasonic S ultrasonic bath (Germany) was used to facilitate the dissolution and dispersion of OV-POSS and SH-POSS in ethanol. Ultrapure water used throughout all experiments was obtained from a ZU101-C ultrapure water system (Zolalan Company, Iran). The water contact angle (WCA) was measured using a goniometer (DataPhysics OCA 15 Plus, Germany) with a droplet volume of 4 μL under ambient conditions. Solution pH adjustments were performed using a Metrohm E520 pH meter (Herisau, Switzerland). The vortex-assisted desorption of MPs was performed using a Heidolph shaker and mixer (Schwabach, Germany). The sorption experiments were monitored using a Cyberscan IR TB100 turbidimeter (EUTECH Instruments, Singapore), with adsorption carried out using a magnetic stirrer-heater. Radiation grafting of POSS on melamine sponge surfaces was achieved *via* UV irradiation using a homemade 265 nm UV LED system (12 V, 5 A for 2 h). The X-ray diffraction (XRD) patterns were obtained using a PANalytical X'Pert PRO MPD X-ray diffractometer. Compression tests were carried out using a universal testing machine (Hounsfield H10Ks, USA) to evaluate the mechanical strength of the samples.

2.3 Synthesis of POSSs

POSS-SH was synthesized through the hydrolysis and condensation of (3-mercaptopropyl)trimethoxysilane (MPTS or 3-MPTMS) under acidic conditions. An amount of 5 mL of MPTS was added to 120 mL of MeOH together with 10 mL of concentrated hydrochloric acid in a three-necked flask equipped with a reflux condenser and magnetic stirring. The mixture was refluxed or stirred vigorously at 90 °C under a nitrogen atmosphere for 24 h, resulting in a white precipitate. The crude product was collected by filtration and subjected to repeated washing steps with MeOH to remove impurities. The viscous intermediate was then dissolved in dichloromethane (CH_2Cl_2), washed multiple times with deionized water, dried over anhydrous Na_2SO_4, and concentrated by rotary evaporation to yield the final POSS-SH product with yields up to 87%.[33,34]

Octavinyl-POSS (OV-POSS) was synthesized following modified procedures reported previously. In a typical synthesis, vinylmethoxysilane (33.32 g) was dissolved in 338 mL of acetone in a flask equipped with magnetic stirring. A mixture of concentrated hydrochloric acid (57 mL) and deionized water (65 ml) was added dropwise to the reaction mixture, which was then refluxed at 40 °C for 48 h. During this time, a white solid precipitated on the flask walls while the solution color changed to brown. The crude product was separated by centrifugation, washed with ethanol, and dried under vacuum at 60 °C. The white powder was further purified by recrystallization from dichloromethane and acetone mixtures (1 : 3 volume ratio).[35,36]

2.4 Sponge pretreatment

Melamine sponges were cut into $1 \times 1 \times 1$ cm^3 cubes, subjected to ultrasonic cleaning in acetone and ethanol to eliminate organic residues, and then dried at 70 °C. For hydroxyl functionalization, sponges were further soaked in a 2.5 mol L^{-1} sodium hydroxide solution for 15 min, enhancing surface reactivity for subsequent coating steps. These pretreatment procedures ensured consistent surface conditions suitable for sol–gel deposition and functionalization, as illustrated in Fig. 1.

2.5 Synthesis of the highly hydrophobic melamine sponge (POSS-MS)

The sol–gel synthesis was carried out using four different amounts of precursor concentrations by adding 1, 2, 3, and 4 mL of 3-(trimethoxysilyl)-1-propanethiol to 50 mL of deionized water, followed by stirring until a clear solution was obtained. After 24 h, 1 mL of ammonia was introduced to initiate gelation; simultaneously, the pretreated sponge was immersed in the solution for 3 h and subsequently heated at 80 °C for one hour. SEM images (Fig. S1) were taken at each stage corresponding to the different precursor concentrations to investigate the morphological evolution of the surface. Among them, the sample synthesized with 2 mL of 3-(trimethoxysilyl)-1-propanethiol exhibited the most uniform and well-distributed coating, with minimal agglomeration and sufficient surface coverage. Therefore, the concentration of 2 mL was selected as the optimal condition for further modifications.

The resulting SH-MS was washed four times with ethanol and dried at 55 °C for 6 h. Then, to functionalize the SH-MS with POSS, the modified MS was immersed in a solution of OV-POSS : SH-POSS and exposed to UV light at 365 nm for 2 h, followed by washing with ethanol and drying at 60 °C. To investigate the influence of feed composition on surface properties, a series of samples were prepared using varying amounts of OV-POSS and SH-POSS (10, 20, 40, and 60 mg) dissolved in 10 mL of ethanol with ultrasonic assistance to promote dissolution and dispersion, maintaining a 1 : 1 mass ratio between the two components. This systematic variation allowed for the evaluation of the effect of POSS content on the resultant surface characteristics. Fig. 2(A)–(C) illustrates that the surface hydrophobicity increased with POSS content up to 40 mg, in which the maximum contact angle ($\sim 152.3^\circ \pm 3.2$) was observed. A further increase to 60 mg did not enhance the hydrophobicity, indicating that 40 mg is the optimum concentration. The WCA of the modified sponges was measured at three different locations on the surface, and the average of these measurements was reported as the final contact angle.

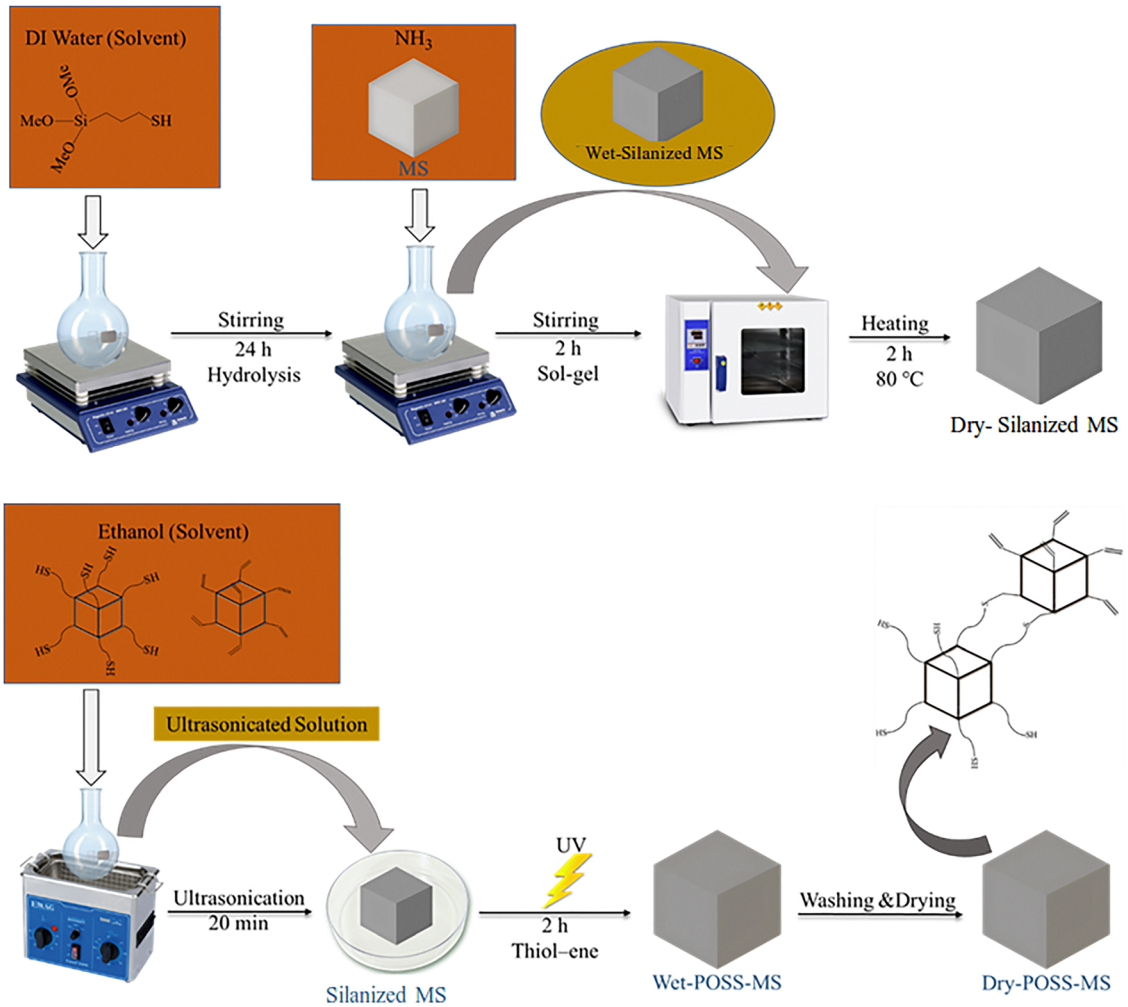

Fig. 1 Preparation processes of the superhydrophobic POSS-MS.

2.6 Removal of the MPs and oil absorption using the POSS-MS

The modified sponge was immersed in 20 mL glass vials containing aqueous solutions (10 mL) of varying PS and PVC MP concentrations at dosages of 100, 200, 300, 400, 500, and 600 mg L^{-1}. The mixtures were maintained on a magnetic stirrer at 25 °C and 100 rpm. Samples were collected at predetermined time intervals (5, 10, 15, 20, 25, 30, 35, 40, 45, 50, 55, and 60 min) to evaluate the adsorption kinetics. In addition, the effect of solution pH on MP adsorption was examined by adjusting the pH to 3, 5, 7, 9, and 11, using 0.1 mol L^{-1} sodium hydroxide or 0.1 mol L^{-1} hydrochloric acid. The concentration of MPs in solution before and after the adsorption experiments was quantified by the turbidity assessment of the supernatant at each time point using a turbidimeter. The removal efficiency was calculated by comparing the MP concentration in solution before and after the adsorption process. The absorption performance of the prepared sponge was evaluated for various oils and organic solvents using gravimetric analysis. For oil and solvent tests, the sponge sample was immersed in 10 mL of the target liquids selected, toluene, *n*-dodecane, kerosene, cooking oil, *n*-hexane, and carbon tetrachloride, at room temperature until fully saturated. After immersion for 1 min, the sponge was removed, drained for 5–10 seconds to eliminate excess liquid, and immediately weighed. All experiments were performed in triplicate, and the average values were reported. The absorption capacity (Q) was calculated using the following equation:

$$\text{Absorption capacity} = \frac{m_c - m}{m}$$

where m_c (g) is the mass of the sponge after absorption, and m (g) is the initial dry mass of the sponge.

2.7 Reusability

The reusability of the modified sponges and functional materials was systematically evaluated through repeated adsorption–desorption cycles. For oils and organic solvents, a repetitive absorption–squeezing process was employed: the sponge was first saturated by immersion in the target oil or solvent, followed by manual squeezing until no visible liquid remained, thoroughly washed with ethanol, dried in an oven, and the cycle was repeated. Sorption capacity was recorded across

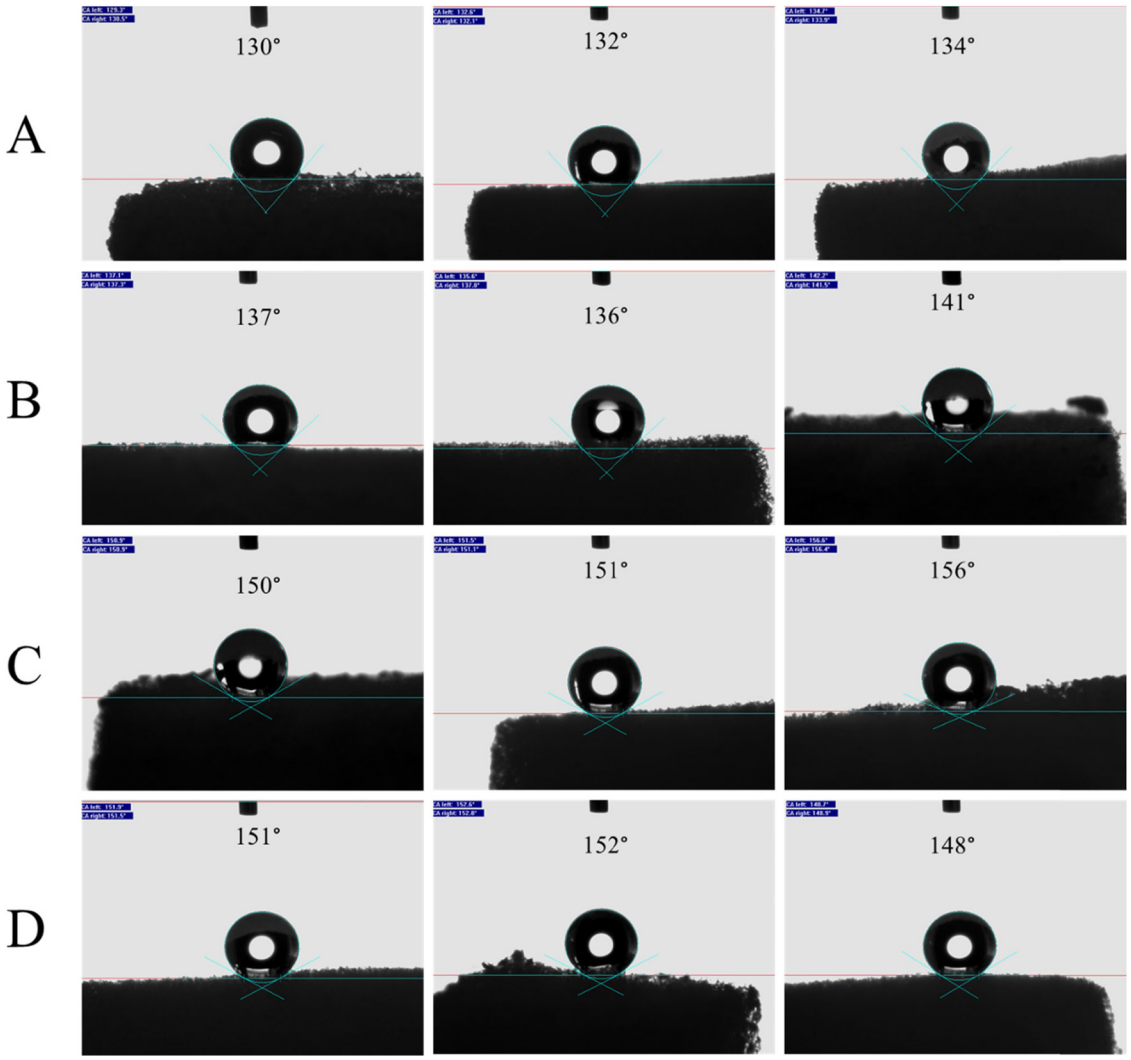

Fig. 2 Water contact angles of the adsorbent surface with varying amounts of OV-POSS and SH-POSS (10 (A), 20 (B), and 40 mg (C)) and WCA of POSS-MS after the adsorption/desorption process (D), each measured at three different surface positions.

10 consecutive cycles. For MPs, the sponge was first saturated by immersion in MP suspensions and then transferred to a glass vial containing 5 mL of ethanol, where the adsorbed analytes were eluted *via* vortex-assisted desorption. The adsorption–desorption cycle was repeated nine times, with the adsorbed analyte quantified after each cycle.

2.8 Sorption kinetics

The experimental data obtained from the adsorption kinetics were examined using the pseudo-first-order (PFO), pseudo-second-order (PSO), and Weber–Morris intra-particle diffusion (IPD) kinetic models, and Avrami fractional-order model. To better demonstrate the extent of fitting between the experimental data and model predictions, statistical error functions (chi-square (χ^2) and root mean square error (RMSE)) were calculated using eqn (5) and (6), respectively. Additionally, the correlation coefficient (R^2) was employed to evaluate the degree of agreement between predicted and experimental results. The model exhibiting the highest R^2 and the lowest χ^2 and RMSE values was considered to provide the best fit.[37]

$$\text{PFO: } \ln(q_e - q_t) = \ln q_e - k_1 t \quad (1)$$

$$\text{PSO: } \frac{t}{q} = \frac{1}{k_2 q_e^2} + \frac{t}{q_e} \quad (2)$$

$$\text{IPD: } q_t = k_{id} t^{0.5} + C \quad (3)$$

$$\text{Avrami: } q_t = q_e[1 - e^{-(k_t)n}] \quad (4)$$

$$\chi^2 = \sum \frac{(q_{exp} - q_{cal})^2}{q_{cal}} \quad (5)$$

$$\text{RMSE} = \sqrt{\frac{1}{n-1}\sum (q_{exp} - q_{cal})^2} \quad (6)$$

In these equations, q_e (mg g^{-1}) denotes the amount of MPs adsorbed at equilibrium, while q_t (mg g^{-1}) represents the amount adsorbed at any given time. The constants k_1 (1 min^{-1}),

k_2 (g mg^{-1} min^{-1}) k_{id} (mg g^{-1} min$^{-1/2}$) and k_{Avrami} (min^{-1}) are the adsorption rate constants for the PFO, PSO, IPD, and Avrami kinetic models, respectively. q_{exp} is the experimental adsorption capacity and q_{cal} is the calculated adsorption capacity.

2.9 Sorption isotherms

To better understand the adsorption behavior and mechanisms of MP adsorption, various isotherm models including Langmuir, Freundlich, Temkin and Sips were applied to experimental equilibrium data. The Langmuir model describes the adsorption of molecules on a homogeneous surface, where a monolayer forms, indicating that all adsorption sites have the same energy and are equally accessible, while for the Freundlich model, multilayer adsorption on heterogeneous surfaces is a favorable route.[38] In the Sips isotherm model, aspects of the Langmuir and Freundlich models are combined, describing multilayer adsorption which is one of the most applicable three-parameter isotherms for monolayer adsorption.[39] The Temkin isotherm model accounts for indirect interactions between the sorbate and sorbent and assumes that the adsorption energy decreases with surface coverage during chemisorption.[38] The fitting models were evaluated by comparing the correlation coefficient (R^2), which reflects the agreement between the predicted values from the sorption models and the experimental data. For this, batch sorption experiments (in triplicate) were conducted using six different initial MP concentrations of 100, 200, 300, 400, 500, and 600 mg L^{-1} and a constant ambient temperature of 25 °C at a neutral pH value of ~8. The fitting parameters for each sorption model are provided in Table S1. These parameters include q_{max} (mg g^{-1}), the Langmuir saturated sorption capacity corresponding to full monolayer coverage; C_e (mg L^{-1}), the equilibrium concentration of MPs in solution; and b, the Langmuir sorption constant, which is related to the energy of sorption (L kg^{-1}). Additionally, k_f (L kg^{-1}) represents the logarithmic Freundlich sorption coefficient, n is the Freundlich exponent, and k_L (L mg^{-1}) is the Langmuir equilibrium constant. For the Temkin model, b_1 is the activity coefficient (J mol^{-1}), k_t is the constant, and b_s is the Sips isotherm constant associated with the energy of adsorption.

3. Results and discussion

3.1. Characterization of the modified MS

ATR-FTIR was employed to monitor the functional groups of the pristine and modified MS, as shown in Fig. 3. Both spectra exhibit several characteristic peaks for the pristine MS that were located at 3336, 3000, 1600, 1538 and 1338 cm^{-1} corresponding to the N–H vibrations, C=O stretching, C=N stretching, triazine ring and methyl bending respectively.[40,41] For the SH-MS, the appearance of a new peak at 2537 cm^{-1} is attributed to the stretching vibration of the S–H bond. However, in the case of POSS coated MS, this peak is absent due to the polymerization process. In the FTIR spectrum of the POSS-MS, an absorption peak at 808.36 cm^{-1} was observed and the increased

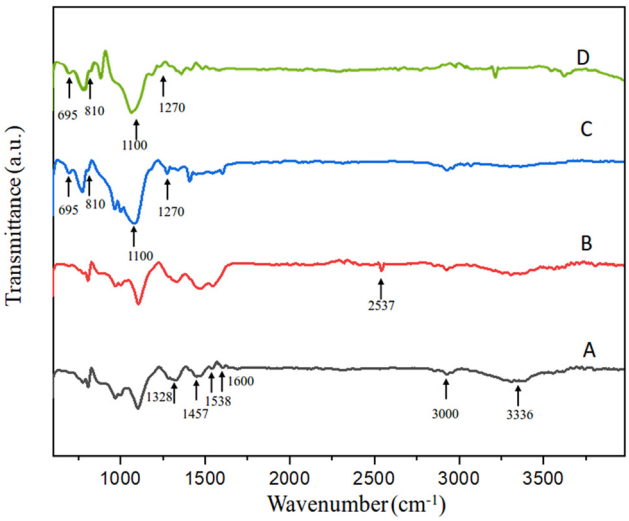

Fig. 3 ATR-FTIR spectra of pristine MS (A), SH modified MS (B), POSS-MS (C), and POSS-MS after the adsorption/desorption process (D).

intensity and sharpness around 1100 cm^{-1} correspond to the symmetric and asymmetric stretching vibrations of the Si–O–Si bonds.[42] The absorption peaks at 695 and 1270 cm^{-1} are attributed to the symmetric and asymmetric stretching vibrations of the Si–C bonds.[27]

The surface morphology of melamine sponges was thoroughly examined using SEM, revealing significant changes following different modification processes. Fig. 4A illustrates that the pristine MS exhibits a characteristic three-dimensional porous structure with a smooth surface texture. As shown in Fig. 4(B) and (C), the entire surface of the SH- and POSS-melamine sponges is covered and their roughness is increased. The modification with POSSs under UV irradiation results in the formation of a new coating layer comparable to the SH-MS surface, where larger surface particles are clearly visible. In the case of POSS-MS, SEM images show a significantly altered surface that imparts a roughened texture, enhancing hydrophobicity due to the low-surface-energy properties of POSS.[43]

Energy-dispersive spectroscopy (EDS) analysis was conducted to confirm the presence and distribution of elements and functional groups on the modified MS surface. The pristine sponge surface primarily contained carbon (C) and oxygen (O), whereas the POSS-modified MS exhibited uniform distribution of additional elements such as silicon (Si) and sulfur (S), indicating successful grafting of POSS onto the MS surface (Fig. S2).

In order to evaluate the surface wettability and hydrophobic properties of the modified and unmodified melamine sponges, water contact angles were measured at three different positions for each sample, and the average values (± standard deviation) are reported. Pristine MS is inherently hydrophilic, rapidly absorbing water upon contact. For instance, the pure MS exhibited a WCA value close to 0°, signifying its strong water affinity. However, surface modification with hydrophobic agents such as SH-POSS and OV-POSS demonstrated significantly improved water repellency. The POSS-MS achieved a

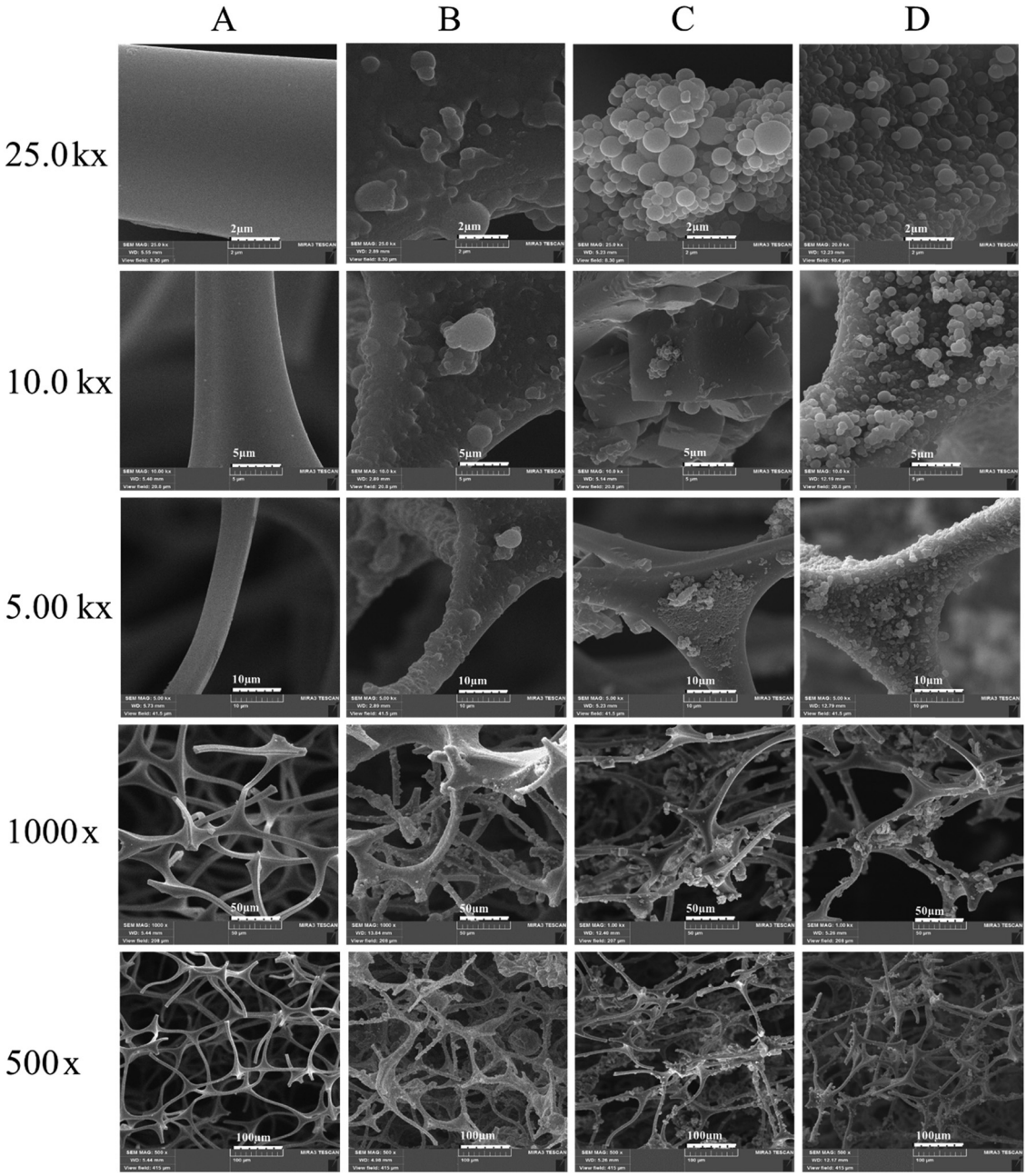

Fig. 4 The SEM images of pristine MS (A), SH coated MS (B), POSS-MS (C), and POSS-MS after the adsorption/desorption process (D).

WCA of 152.3° ± 3.2, confirming that the prepared surface is highly hydrophobic. This surface modification not only enhanced water repellency but also contributed to oil–water separation capabilities.

The modified sponge was able to selectively absorb oil while repelling water. As illustrated in Fig. 5A, *n*-hexane droplets stained with red dye readily permeate and are fully absorbed into the surface of the POSS-modified melamine sponge, indicating strong oleophilicity. In contrast, water droplets stained with methylene blue retain a near-perfect spherical shape on the same surface, highlighting its pronounced hydrophobicity. Moreover, when the sponges are immersed in water, the modified sponge remains buoyant and floats on the surface, whereas the pristine MS rapidly absorbs water and sinks, as shown in Fig. 5B. The modified sponge effectively repels the water stream, preventing any penetration or passage through its structure, whereas the pure sponge readily allows water to infiltrate and flow through due to its inherently superhydrophilic nature (Fig. 5C and D).

Based on the nitrogen adsorption–desorption isotherms and Barrett–Joyner–Halenda (BJH) pore size distribution curves (Fig. S3), the MS and POSS-MS exhibit a Type III isotherm profile with an H_3 hysteresis loop, indicating the contribution of mesoporous and macroporous structures.[44] In this type of isotherm, adsorption at low relative pressures is negligible due

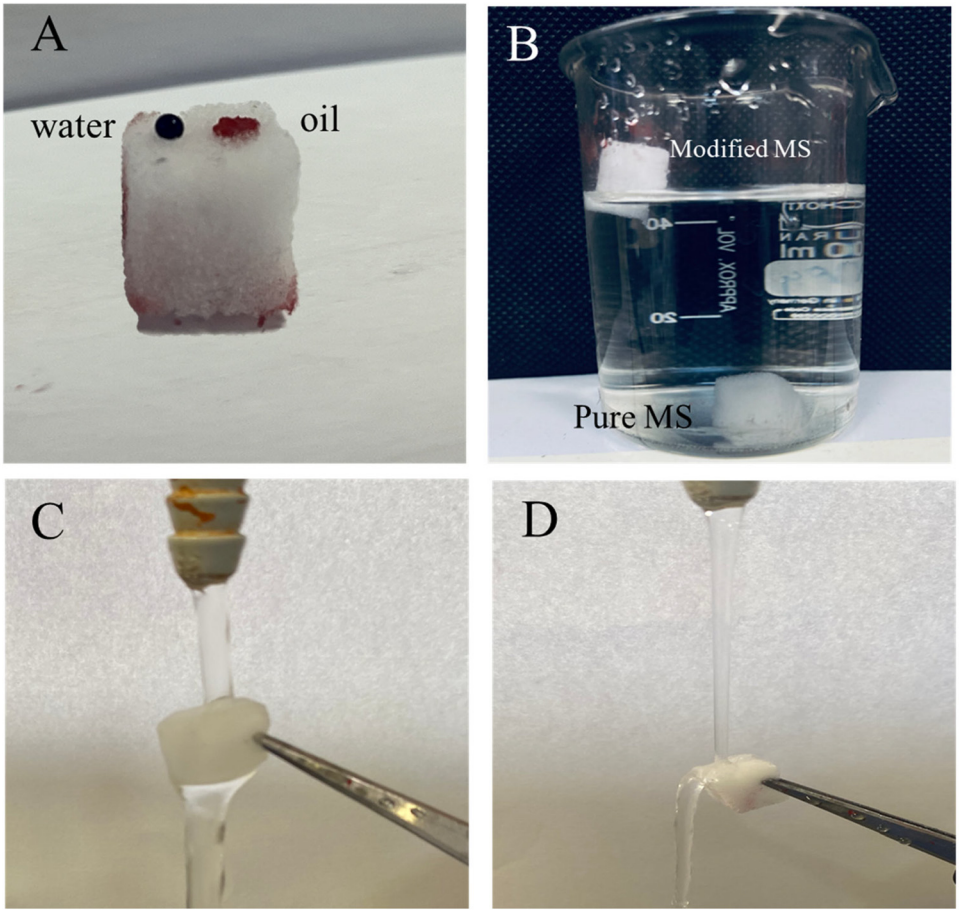

Fig. 5 Wetting behavior of POSS-MS to oil and water (A). Floating behavior of pristine and modified sponges in water (B). Comparison of water-repellent properties under water flux: the porous coated sponge exhibits complete water repellency, whereas water readily passes through the pure sponge (C) and (D).

to the weak interaction between the adsorbate and the adsorbent surface, while a sharp increase in adsorption at high relative pressures ($P/P_0 > 0.9$) corresponds to multilayer formation. The adsorption mechanism and pore structure remain essentially unchanged before and after modification. The BET surface area, total pore volume, and average pore diameter of the materials are summarized in Table S2.

To evaluate the structural stability of the prepared POSS-MS, several characterization techniques were employed before and after the adsorption/desorption process. As shown in Fig. 4D, the SEM images reveal that the morphology and porous framework of the POSS-MS remained almost unchanged after the use, indicating that the POSS-MS retained its structural integrity without noticeable collapse or deformation. The ATR-FTIR spectra (Fig. 3) of the POSS-MS before and after the adsorption/desorption cycles displayed nearly identical characteristic peaks, confirming that the functional groups were well preserved during the process. In addition, the XRD patterns (Fig. S4-A) exhibited an amorphous silicon peak at approximately 21.3° (2θ). After adsorption, the patterns showed similar shapes without new peaks or position shifts, indicating that no phase transformation occurred. The slight decrease in peak intensity may be attributed to the adsorption of pollutants on the sponge surface; nevertheless, the amorphous framework of the POSS-MS remained unchanged, confirming its structural stability.

The WCA of POSS-MS after being used was 150.3 ± 2.0, and statistical analysis using a t-test ($t = 1.64$, $p > 0.05$) indicated no significant difference compared to the initial value. The structural stability of the sponge was further examined under harsh conditions by immersing it in 0.1 M NaOH solution for 8 h. The WCA values obtained afterward (~150° ± 3.8) demonstrated that the surface hydrophobicity was well preserved (Fig. S4-C).

Mechanical stability was also investigated through compressive stress–strain measurements (Fig. S4-B). The curves illustrate the mechanical behavior of the modified sponge during 20 successive compression–release cycles. At strains below 10%, the sponge shows a linear elastic region related to the bending of pore walls, followed by a deformation plateau (20–70% strain) attributed to elastic buckling. At higher strains (>75%), a densification region appears, where stress rises sharply due to the collapse and close contact of cell walls.[45] After 20 cycles, the stress–strain curves gradually shift upward, indicating a slight enhancement in stiffness, likely due to minor pore compaction.

However, the overall curve shape remains nearly unchanged, suggesting no significant loss of elasticity. These results confirm that the modified sponge exhibits sufficient mechanical flexibility and structural resilience, maintaining its three-dimensional framework even after repeated compression.

Taken together, the morphological, structural, and mechanical results confirm that the POSS-MS possesses high structural stability and durability. The strong bonding between the melamine sponge and the POSS framework ensures good recyclability and suitability for practical applications such as contaminant removal and oil cleanup, even under harsh environmental conditions.

3.2. Sorption kinetics

Experimental data were collected at various time intervals to examine the rate-controlling processes, using four different kinetic models: pseudo-first-order, pseudo-second-order, Avrami fractional, and intraparticle diffusion models. As shown in Fig. 6A and B, the adsorbed amount of PVC and PS MPs approximately increased rapidly in the first 30 min and then gradually reached equilibrium after 45 min. This rapid increase can be attributed to the mass transfer driving force created by the initial concentration gradient between the sponge and water, coupled with the abundant adsorption sites on the MS surface. Based on the results mentioned above, a contact time of 45 min was selected for the MP removal experiments. Fig. 6(C) and (D) compares the equilibrium experimental and theoretical adsorption capacity values of each MP, demonstrating that, for both PS and PVC, the pseudo-second order kinetic model offers a reasonably good fit of the experimental data. Fig. S5 and S6 display the results of the adsorption kinetic models of MPs, while Table 1 and Table S3 provide the detailed kinetic parameters together with the corresponding correlation coefficient R^2, RMSE, and χ^2 values for each kinetic model. For the pseudo-first-order model, the poor fitting of the model can be attributed to its inherent assumption that the adsorption rate depends solely on the number of unoccupied sites. In the present system, the adsorption rate is influenced not only by available sites but also by physicochemical interactions between the MPs and the POSS-MS. The correlation coefficients are fairly low lying between 0.83 and 0.91. As presented in Table S3, the calculated kinetic parameters indicate that among the three examined models, the pseudo-second-order model provides the best overall agreement with the experimental data, as evidenced by its highest correlation coefficient ($R^2 \geq 0.96$), lowest χ^2 and RMSE values. These results confirm a strong consistency between the experimental data and the pseudo-second-order

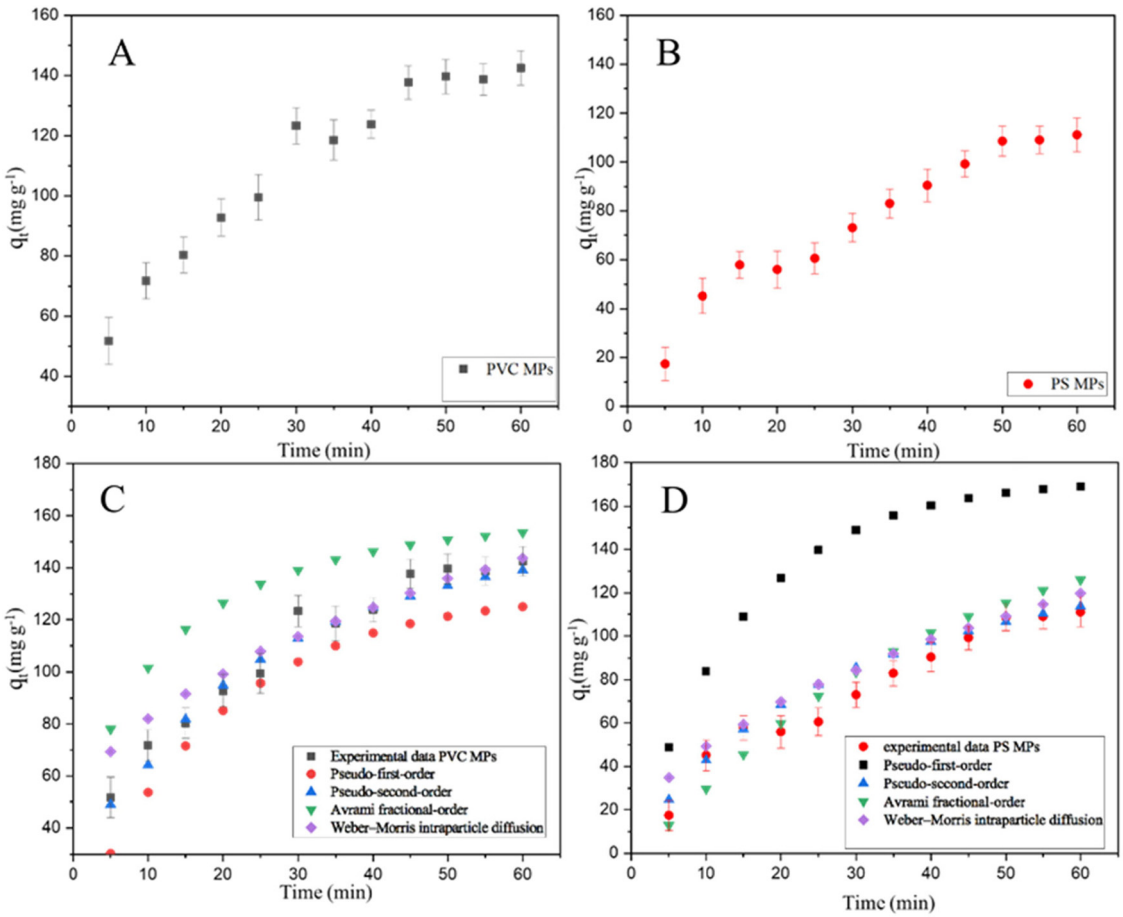

Fig. 6 Sorption capacity of PVC (A) and PS (B) MPs on POSS-MS; comparison of experimental and theoretical adsorption capacities of PVC (C) and PS (D) MPs.

Table 1 Kinetic parameters for the MP adsorption by the POSS-MS

	Pseudo-first-order			Pseudo-second-order			Avrami fractional-order			Weber–Morris intra-particle diffusion		
MPs	k_1 (min^{-1})	q_e (mg g^{-1})	R^2	k_2 [g (mg $min)^{-1}$]	q_e (mg g^{-1})	R^2	k_A [min^{-1}]	n	R^2	k_{id} (mg g^{-1} $min^{-1/2}$)	C	R^2
PVC	0.070	165.181	0.91	3×10^{-4}	181.81	0.98	0.0833	0.709	0.74	13.6	39.14	0.86
PS	0.066	170.21	0.83	2×10^{-4}	169.49	0.96	0.0423	1.33	0.91	17.29	18.89	0.96

kinetic model. The results from the pseudo-second-order model indicate that the adsorption process is mainly governed by chemisorption involving surface interactions between the hydrophobic POSS-MS and the PS/PVC MPs. This model highlights that the adsorption process is influenced by both time and binding site availability of the modified sponge.[46,47] As expected, the Avrami kinetic model exhibited R^2 values of 0.74 and 0.91 for PVC and PS, respectively. These data can be attributed to the fact that this model is primarily developed for phase transformation.[48]

The adsorption process of PS MPs onto the POSS-sponge can be described using the Weber–Morris IPD model, which revealed that the PS adsorption process occurs in three distinct stages (Fig. S6-D); however, the intercept position indicates that the adsorption process is controlled by multiple mechanisms.[49] The adsorption rate constants follow the order k_{i1} (29.41 mg g^{-1} $min^{-1/2}$) > k_{i2} (20.18 mg g^{-1} $min^{-1/2}$) > k_{i3} (3.8 mg g^{-1} $min^{-1/2}$), revealing a gradual rate decrease over time. The initial sharp region (k_{i1}) lasting for about 15 min is attributed to the rapid migration of PS MPs from the solution to the sponge surface through boundary layer diffusion and surface adsorption. During the second phase (~15–45 min), the adsorption rate decreases, indicating that the process is governed by pore diffusion, as PS migrates into the interior adsorption sites of the adsorbent. The gradual stage continues until most of the internal pores become occupied.[50,51] In the final stage, the adsorption rate further declines and eventually reaches equilibrium, primarily due to the limited active site availability and the reduced PS concentration in the solution.

3.3. Sorption isotherm

As shown in Fig. S7 and S8, adsorption isotherms were fitted to obtain a mechanistic understanding of the adsorption processes for MPs. The equilibrium adsorption concentration of MPs increases with the initial concentration, indicating a non-uniform distribution of adsorption sites on the adsorbent surface, which is characteristic of multilayer adsorption. As shown in Table 2, after fitting the Freundlich isotherm model, the R^2 values obtained for the MP adsorption were 0.9600, suggesting the presence of a heterogeneous surface, while other models such as Temkin and Sips exhibited $R^2 < 0.91$ and were therefore not considered. In the Freundlich isotherm model, the n_F value reflects the heterogeneity of the POSS-MS surface. In this study, the n_F values were 1.05 and 2.18 for PS and PVC MPs, respectively, demonstrating that the adsorption process is favorable.[52] This model is nonlinear and reflects surface heterogeneity, where both physical and chemical adsorption contribute to the adsorption of MPs.[53] The assumption of multilayer adsorption on heterogeneous surfaces with varied energy distribution contrasts with the Langmuir model's concept of monolayer adsorption, highlighting the complexity of interactions during the sorption process. As the k_F value increases, the removal efficiency generally improves, reflecting a stronger affinity of MPs for the POSS-MS surface. In the Freundlich model, k_F represents the adsorption affinity coefficient and indicates how strongly the adsorbent interacts with the adsorbate.[54] A comparison of the data shows that $k_{F,PVC} > k_{F,PS}$, suggesting that the POSS-MS has the highest affinity toward PVC MPs, followed by PS. Additionally, as shown in Fig. 7, the Freundlich isotherm model provides a better prediction of the adsorption capacities, with the calculated values being very close to the experimental results for both PVC and PS MPs.

3.4. Salinity effect

Given the high prevalence of various ions in natural aquatic environments such as rivers, lakes, and oceans, it is essential to investigate their impact on the removal efficiency of MPs. Specifically, the ionic strength and presence of common salts such as NaCl, KCl, and $CaCl_2$, which are possible coexisting species, were systematically evaluated in this study. To this end, three concentration ranges of calcium, sodium, and potassium salts were employed to assess their influence on the adsorption efficiency of the introduced adsorbent, thereby providing insights into the role of ionic composition on MP adsorption in natural water systems. Fig. 8(A) and (B) shows the effect of NaCl, $CaCl_2$ and KCl on the MP removal. As illustrated, the MPs' removal efficiency increased with rising concentrations of calcium ions, whereas the variations in potassium and sodium ion concentrations had no significant effect on the removal rate. The presence of divalent Ca^{2+} cations in the solution exerts a bridging effect between the negatively charged surfaces of MPs and the adsorbent, thereby facilitating sorption and

Table 2 Adsorption isotherm (Langmuir, Freundlich, Temkin, and Sips) constants for the MP adsorption

	Langmuir			Freundlich			Temkin			Sips		
MPs	q_{max}	k_L (L mg^{-1})	R^2	k_f (L kg^{-1})	n	R^2	b_1	k_t	R^2	S	b_s	R^2
PVC	250	0.001	0.87	14.96	2.18	0.96	41.37	0.27	0.85	1.28	0.37	0.63
PS	1428.57	0.0007	0.13	1.18	1.05	0.96	75.32	0.04	0.91	0.51	0.01	0.86

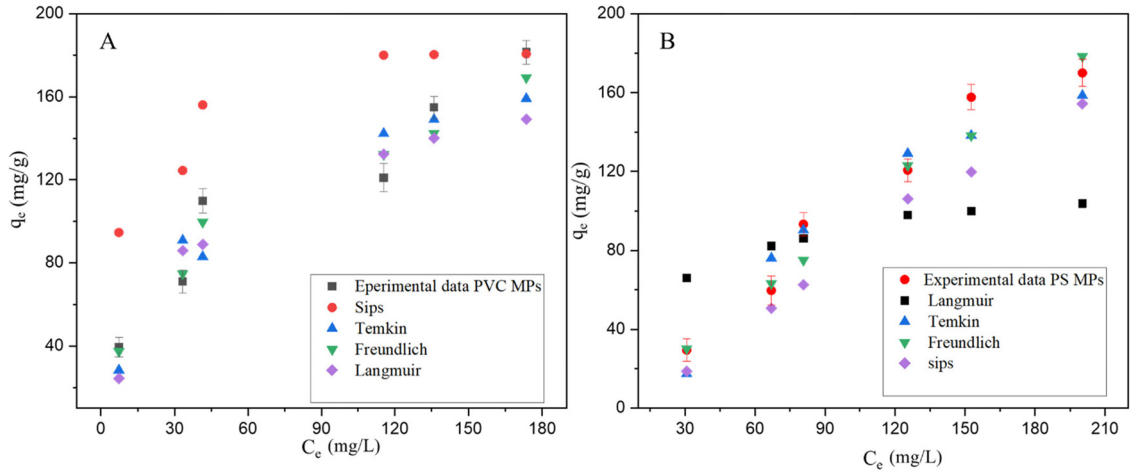

Fig. 7 Comparison of experimental and theoretical equilibrium data of PVC (A) and PS (B) MPs fitted by isotherm models.

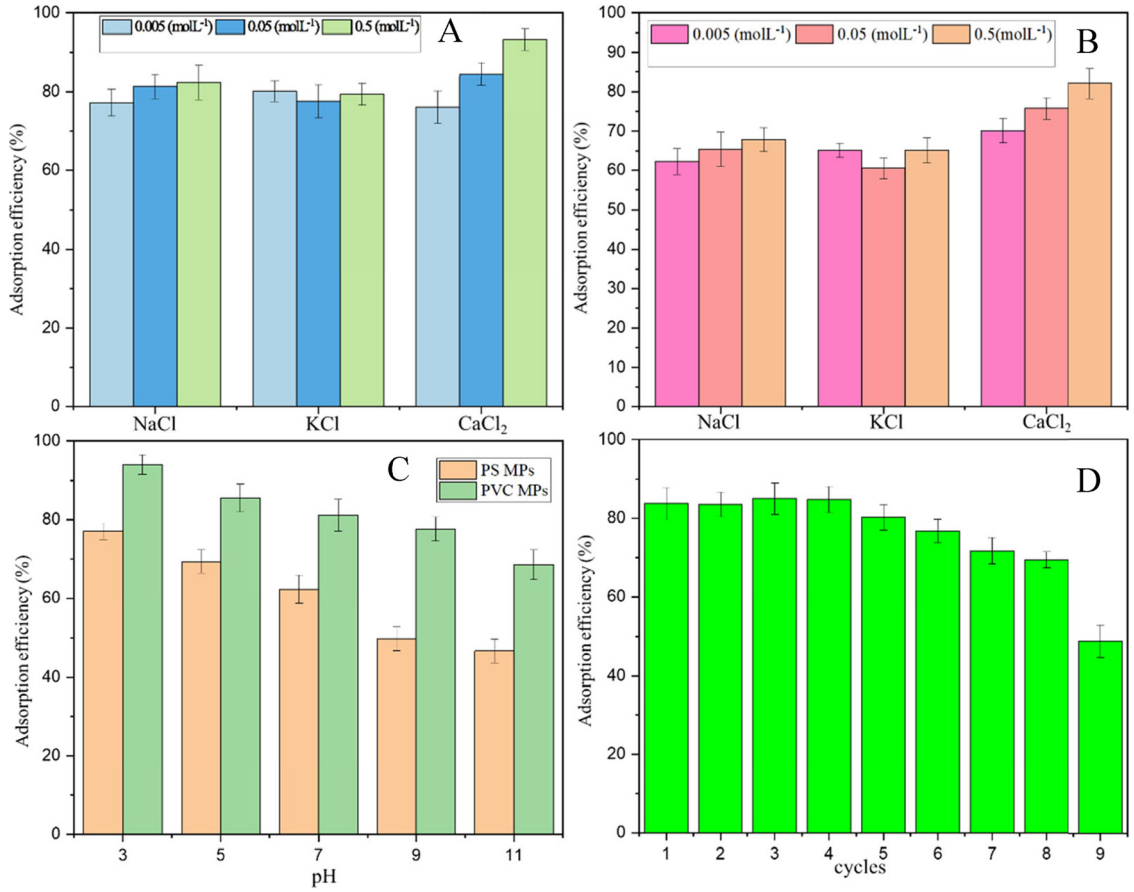

Fig. 8 Effect of salinity on sorption of MPs by POSS-MS: PVC MPs (A) and PS MPs (B), effect of solution pH (C), and adsorption–desorption performance over nine cycles (D).

enhancing the removal efficiency of MPs.[55] In contrast, monovalent cations such as Na^+ and K^+ exhibit negligible influence on the adsorption capacity. Consistent with these findings, the current study observed that calcium ions markedly enhanced the removal efficiency of MPs by increasing adsorption rates, whereas sodium and potassium ions had an insignificant effect. This enhancement is attributed to the ability of bivalent calcium to act as an electrostatic bridge, overcoming the mutual repulsion between the negatively charged adsorbent and MP surfaces.

3.5. pH effect

As shown in Fig. 8C, the adsorption efficiency of MPs onto the POSS-MS varies with pH due to changes in zeta potential, decreasing from 94.4% and 77.12% at pH 3 to 68.7% and 46.67% at pH 11 for PVC and PS MPs, respectively. At pH 3, PS and PVC MPs exhibit positive surface charges (8 and 14 mV, respectively), while the POSS-MS carries a weakly negative charge (−4.6 mV), as shown in Table 3, which reduces electrostatic repulsion and promotes strong adsorption. However, as the pH increases, both the MPs and the POSS-MS become negatively charged as indicated by their increasingly negative zeta potentials at pH 7 and pH 11 (−3.6 to −4.8 mV for PS MPs, −8.5 to −48.1 mV for PVC MPs, and −1.1 to −8 mV for the POSS-MS) leading to enhanced electrostatic repulsion and a significant decrease in removal efficiency. According to Table 3, this clear shift toward more negative surface charges with increasing pH explains the observed reduction in the amount of adsorbed MPs under alkaline conditions. Notably, the POSS-MS demonstrated exceptional adsorption capacity for PS and PVC MPs across a wide pH range, highlighting its versatility as an effective removal platform.

3.6 MP removal mechanism

The removal of MPs by adsorbent materials is governed by the interplay of physical and chemical interactions, influenced not only by the inherent properties of the MPs and the characteristics of the adsorbent but also by extrinsic environmental and biological conditions. Together, these factors determine the adsorption affinity, mechanisms, and overall efficiency of MP removal from aqueous systems.

Specifically, the removal of MPs by modified sponge involves several mechanisms. Capillary action, arising from the abundant three-dimensional porous structure of the sponge, effectively attracts and retains MP particles suspended in water. Physical adsorption of hydrophobic MPs is further facilitated by the highly hydrophobic surfaces of the POSS-MS, in which hydrophobic interactions play a central role in the rapid migration and accumulation of MPs at the adsorbent interface. The availability and distribution of sorption sites on the sponge surface are critical in dictating the initial fast uptake, as MPs migrate toward the POSS-MS from the aqueous phase. For PS, π–π interactions, non-covalent attractions between the aromatic rings of the polymer and the π-system of the double bond present on the POSS-MS, significantly enhance adsorption efficiency. Halogen bonding may also play a role in PVC MPs, where interactions occur between Cl atoms and the π-electrons of the adsorbent double bond. The slightly positive surface charge of MPs under acidic conditions promotes electrostatic attraction toward negatively charged POSS-MS, enhancing the adsorption efficiency. The combined effect of these mechanisms, including capillary action, hydrophobic interactions, π–π interactions, and halogen bonding, makes this highly hydrophobic sponge a favorable platform for the removal of diverse MPs from water. The removal of MPs by POSS-MS is illustrated in Fig. S9, showing the suspensions of PS and PVC MPs before and after removal.

Table 3 Zeta potential of MPs and POSS-MS at different pH levels

	Zeta potential		
Sample	pH 3	pH 7	pH 11
PS MPs	8 mV	−3.6 mV	−4.8 mV
PVC MPs	14 mV	−8.5 mV	−48.1 mV
Adsorbent	−4.6 mV	−1.1 mV	−8 mV

During the desorption process, the weak and reversible non-covalent interactions responsible for MPs' adsorption such as hydrophobic interactions, van der Waals forces, and π–π stacking can be easily disrupted through simple mechanical squeezing and rinsing with ethanol or water. The efficient release of MPs confirms that the adsorption mechanism is predominantly dominated by a physical process.

3.7 Evaluation of MPs removal by POSS-MS in river and sea water

The compatibility of the developed method for analyzing MPs in real water matrices was assessed using river and sea water as representative of environmental samples. Both water matrices were spiked with MPs at a concentration of 400 mg L^{-1}, and the observed removal efficiencies were comparable to those obtained using Milli-Q water, indicating negligible matrix effects. Prior to experimentation, the water samples were filtered through a 0.45 μm membrane to remove suspended solids and subsequently characterized for water quality. Comparative studies revealed that all quantified MPs originated solely from the spiked real water samples. At pH 3, identified as the optimal condition for MP removal in Milli-Q water, the removal efficiency in seawater reached ∼94%, while at the normal pH, the efficiency was around 88%. Similarly, the removal efficiency in river water at pH 3 was 89%. Notably, the prepared POSS-MS exhibited high efficiency in removing MPs from seawater containing multiple high-concentration ions. These findings suggest that the modified sponge exhibits excellent potential for practical applications in MP removal and water treatment.

3.8 Oil sorption properties of the POSS-MS

The oil sorption performance of the modified sponge highlights the critical influence of surface chemistry, porosity, and physicochemical interactions on the target liquids. Experimental results involving both floating and submerged oils demonstrate that the highly hydrophobic nature of the POSS-MS enables selective sorption of oils and organic liquids with higher and lower densities than water, such as carbon tetrachloride (CCl_4) and toluene, as shown in Fig. 9(C) and (D). This selective sorption, without any water uptake, is attributed to the sponge's three-dimensional porous structure and the capillary-driven mechanism facilitating oil uptake from both above and below the water surface. The sorption capacity of the modified sponge exhibited significant variation depending on the type of oils and organic solvents, which were selected as model absorbates based on their density. As shown in Fig. 9A, the capacity

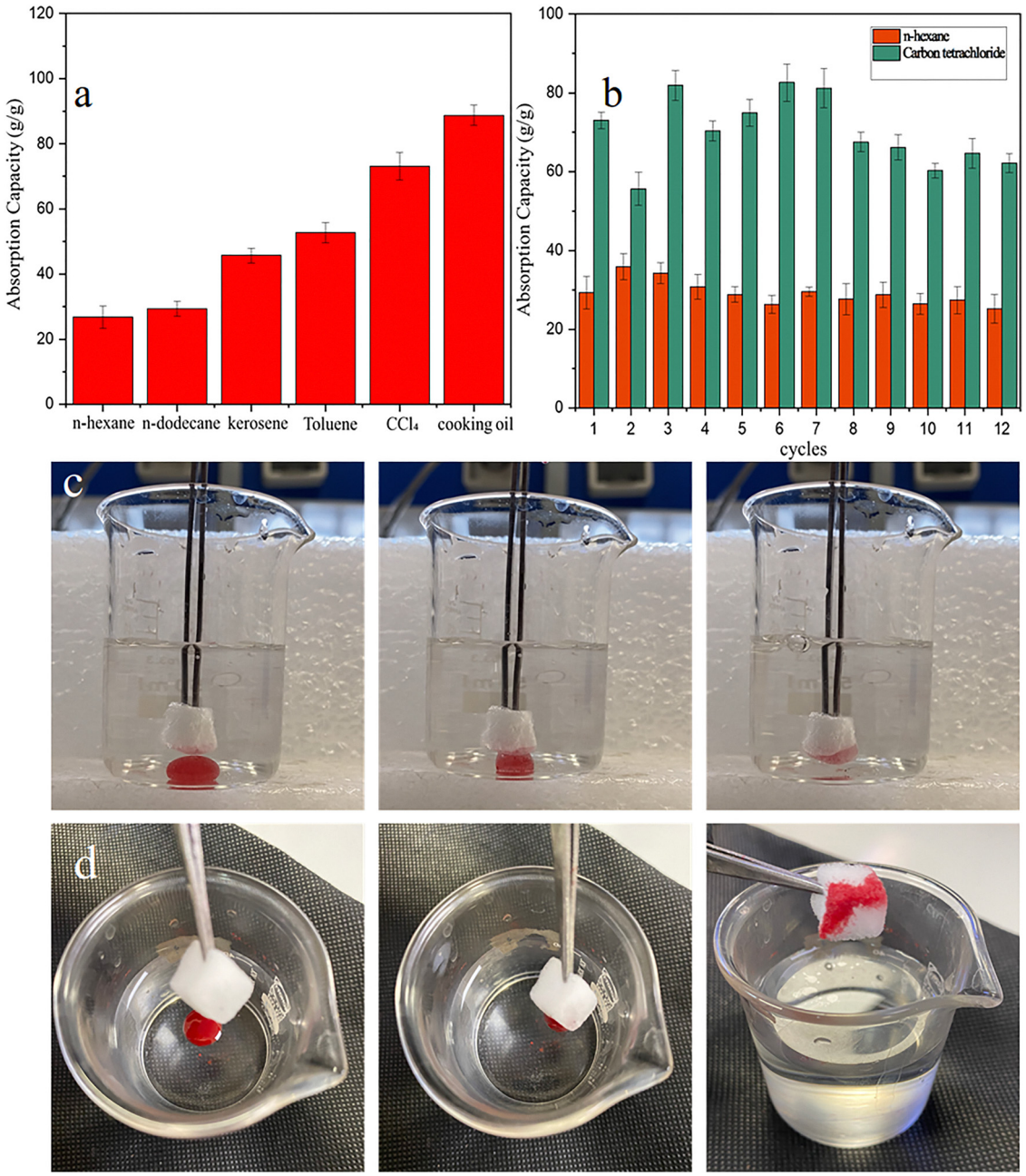

Fig. 9 Maximum absorption capacities of the POSS-MS for various organic liquids (A) and absorption recyclability of the sponge for model organic liquids (*n*-hexane and carbon tetrachloride) over 12 absorption–squeeze cycles (B). Optical photographs demonstrating carbon tetrachloride absorption under water (C) and *n*-hexane absorption on the water surface using the POSS-MS sponge (D) (oil and organic solvent phase colored with red dye).

ranged from 27 to 89 g g^{-1} and followed the increasing order: *n*-hexane < *n*-dodecane < kerosene < toluene < CCl_4 < cooking oil. This trend reflects the combined effects of the liquids' density and viscosity on the sponge's absorption behavior. Although cooking oil has a lower density (0.91 g cm^{-3}) than carbon tetrachloride (CCl_4, 1.59 g cm^{-3}), it exhibited a higher adsorption capacity, indicating that factors beyond density influence the absorption performance. This deviation from the expected density–capacity relationship is attributed to the swelling behavior of the sponge upon exposure to cooking oil. The interaction between the sponge matrix and the viscous oil likely induces volumetric expansion, thereby increasing the effective void volume available for absorption and enhancing the overall capacity.[56] A similar phenomenon has been reported for other porous sponges such as graphene oxide and reduced graphene oxide coated polyurethanes, which absorbed more tetrahydrofuran (THF) than dimethyl sulfoxide (DMSO), even though THF has a lower density.[57] The POSS-MS demonstrates comparable or enhanced oil and organic solvent absorption and MP adsorption relative to various previously reported porous sorbents, as summarized in Table 4.

Table 4 Comparison of superhydrophobic sponge-based materials for oil absorption and MP removal[a]

Adsorbent	Adsorption/absorption conditions	Pollution	Maximum MP removal efficiency and saturated oil absorption capacity	Ref.
Oat protein sponge	pH range = 6–9 with an initial microplastic concentration of 1 mg L^{-1}. Time = 1, 2, 4, 6, 8, 11, and 24 h.	PS MPs	81.2%	10
Chitin-GO sponge	pH = 6–8. MP concentration of 1 mg L^{-1}. Time = 1, 2, 3, 5, 7, 9, 12, and 24 h.	PS MPs	89.8%	58
GO/chitosan/genipin sponge	pH range = 5.5–10.0. MP concentration of 1 mg L^{-1}. Time = 0.5, 1, 2, 4, 8, 12, 36, and 48 h.	PS MPs	41.5%	59
Magnetic sponge carbon	pH = 3–11. MP concentration of 200 mg L^{-1}. Time = 5, 1, 3, 5, 10, 15, and 20 min	PS MPs	0.369 g g^{-1}	60
Sodium alginate sponge	pH = 3, 7, 10. MP concentration of 100 mg L^{-1}. Time = 2.5–35 h.	PS MPs	92.3%	61
Chitin based sponge	MP concentration of 1 mg L^{-1}. Time = 14 d.	PP MPs	71.6–92.1%	62
Superhydrophobic sponge derived from the loofah plant	pH = 6. Concentration of MPs 500 mg L^{-1}. Time = 30 min.	PS MPs	≥99%	63
Chitin-PANI sponge	pH = 4–10. MP concentration of 1 mg L^{-1}. Time = 1, 2, 3, 5, 7, 9, 11, 13, and 24 h.	PS MPs	84–91.7%	64
Starch–gelatin sponge	pH range = 2–11. 40 mL of the MP concentration of 25 mg L^{-1}. Time = 1, 3, 6, 11, 17, 22, and 24 h	PMMA and PS MPs	40–70%	65
POSS-MS	pH = 3–11. MP concentration of 400 mg L^{-1}. Time = 5, 10, 15, 20, 25, 30, 35, 40, 45, 50, 55, and 60 min.	PS and PVC MPs	82–94%	This study
MS-PFOTES	Saturated sorption–squeezing process repeated up to 15 cycles.	Model oil and solvent pollutants	39.3–117.5 g g^{-1}	66
AOS@MMT-PU	Each test oil was added dropwise. Absorption time: a few seconds.	Oils and non-polar organic solvents	29.5–66.5 g g^{-1}	67
MS-METES	30 mL of the test oils and organic solvents. Time: 1 min.	Petroleum products, oils, and organic solvents	49.6–122.4 g g^{-1}	68
CNT reinforced P sponge	Absorbed the oil within five seconds.	*n*-Hexane	34.9 g g^{-1}	69
Chitosan sponge	Immersed in the test oil or solvent at room temperature.	Chloroform	60 g g^{-1}	70
MS-PTES	Saturated sorption–squeezing process repeated up to 15 cycles.	Petroleum products, oils, and organic solvents	47.6–132.2 g g^{-1}	71
ND-ODA@PDMS@MS	The sponge was saturated with organic liquids or oils from oil/water mixtures.	Oils and non-polar organic solvents	26.65–55.64 g g^{-1}	72
THS@MS	Equal drops of each test oil were placed in 50 mL of deionized water.	Oils and non-polar organic solvents	62.03–71.33 g g^{-1}	73
MS-HNT/HDTMS	30 mL of the test oils and organic solvents. Time: 10 min.	Petroleum products, oils, and organic solvents	31.0–90.4 g g^{-1}	74
MS-ZIF-67	Saturated sorption–squeezing process	Chloroform	177 g g^{-1} for	75
UFC foam	Foam immersed in organic liquid for 1 min	Organic solvents and oils	71–158	76
MIL-DDT@MS	Immersed in 10 mL of the test oils and organic solvents until it is fully saturated.	Oil or organic solvents	54.1–120.2 g g^{-1}	77
Sn-PBZs	Oil-absorbing bag consisting of a nylon sheath with SnPBZ filler.	Diesel as crude oil	10.08 g g^{-1}	78
OV-POSS@MS	Submerged in different solvents and fully absorbed.	Organic solvents	41–80 g g^{-1}	79
F-POSS-SH@MS	Immersed in organic solvents or oils for 5 min.	Oils and organic solvents	45 to 94.5 g g^{-1}	80
Ph-POSS@HKUST-1@PDA@sponge	Saturated sorption–squeezing process	Oils and organic solvents	18.8–48.3 g g^{-1}	81
O-Ph-POSS-FG@sponge	Saturated sorption–squeezing process	Oils and organic solvents	15–55 g g^{-1}	82
POSS-MS	10 mL of the target. Absorption time: immersion for 1 min.	Oils and non-polar organic solvents	27 to 89 g g^{-1}	This study

[a] Abbreviations: GO, graphene oxide; PANI, polyaniline; PDA, polydopamine; SA, stearic acid; PU, polyurethane; CNTs, carbon nanotubes; NDs, nanodiamonds; ODA, octadecylamine; PDMS, polydimethylsiloxane; THS, trimethoxy silane; PFOTES, perfluorooctyl triethoxysilane; PTES, phenyltriethoxysilane; HNT, halloysite nanotube; METES, methyltriethoxysilane; OTES, octyltriethoxysilane; UFC, ultralight, fire-resistant, and compressible; DDT, dodecanethiol; M-PBZs, metal-polybenzoxazine micro-nano-spheres; OV, octavinyl; and FG, fluorinated graphene.

3.9 Reusability

Reusability is a critical parameter for evaluating the practical applicability and cost-effectiveness of adsorbents in large-scale oil–water separation and MP removal processes. To assess this, a series of cyclic sorption/desorption experiments were conducted on modified sponges. The POSS-MS maintained ~80% MP removal efficiency over the first five cycles and ~68% after eight cycles, indicating good reusability and environmental

friendliness (Fig. 8D). These results demonstrate good reusability and environmental compatibility with only minor declines in adsorption efficiency observed across eight cycles, underscoring its potential for durable MP removal in water treatment.

The reusability performance of the modified sponge for oil absorption was systematically evaluated through 12 sorption/squeezing cycles using *n*-hexane and carbon tetrachloride as model organic solvents (Fig. 9B). The results demonstrate a consistent and stable absorption behavior across cycles for both solvents, highlighting the material's structural robustness and efficient regeneration capacity. For *n*-hexane, the sorption capacity ranged from approximately 26 to 30 g g^{-1} over the ten cycles, with only minor fluctuations and no significant decline. This indicates that the sponge retained its structural integrity and surface properties over repeated use, suggesting strong mechanical durability and solvent compatibility. In the case of carbon tetrachloride, the sponge exhibited higher absorption capacities, between ~63 and 73 g g^{-1}, reflecting the influence of CCl_4's higher density and stronger van der Waals interactions with the hydrophobic sponge matrix. Although some variability is observed in the CCl_4 absorption values (particularly in cycles 2–5), the overall trend remained stable in the latter cycles, suggesting that after initial equilibration or structural adaptation, the sponge maintained its absorption efficiency. These findings confirm the acceptable reusability of the modified sponge for both low- and high-density organic solvents, making it a promising candidate for practical applications in oil spill remediation and organic solvent recovery.

4. Conclusion

This study demonstrates the successful development of a highly hydrophobic POSS-functionalized melamine sponge capable of efficiently removing both MPs and hydrophobic organic pollutants from water. The POSS-MS efficiently removed MPs through physical and chemical mechanisms, including capillary action, hydrophobic interactions, π–π stacking, and halogen bonding. The POSS-MS exhibits high adsorption capacities, rapid kinetics, reaching equilibrium within 45 minutes, and robust performance across a wide range of environmental conditions, including variations in pH and salinity. The MP adsorption is best described by the pseudo-second-order kinetic model, indicating a predominant chemisorption process. Isotherm analysis showed multilayer adsorption on a heterogeneous surface, with Freundlich model fitting and a higher affinity toward PVC over PS. The removal efficiency was significantly enhanced by the presence of calcium ions due to electrostatic bridging, whereas sodium and potassium ions had minimal effect. Although adsorption decreased with increasing pH, the sponge maintained high performance across a broad pH range. Its reusability was confirmed through multiple sorption/desorption cycles, underscoring its potential for practical and sustainable water treatment applications. The findings highlight the promise of POSS-based surface modification as an environmentally friendly approach to fabricating efficient adsorbents for large-scale remediation of aquatic pollutants.

Conflicts of interest

There are no conflicts to declare.

Data availability

Data for this paper are available in the manuscript and its supplementary information (SI). The supplementary information includes detailed experimental procedures, characterization data, and additional figures supporting the main text. See DOI: **https://doi.org/10.1039/d5nj03353e**.

Acknowledgements

Dr Reza Dehbandi of the University of Birmingham, Birmingham is highly acknowledged for providing the PS MPs. This project was supported by the Graduate School and Research Office of Sharif University of Technology (Grant Number QA990417).

References

1 S. M. Mintenig, M. Kooi, M. W. Erich, S. Primpke, P. E. Redondo-Hasselerharm, S. C. Dekker and A. P. Van Wezel, A systems approach to understand microplastic occurrence and variability in Dutch riverine surface waters, *Water Res.*, 2020, **176**, 115723.

2 J. P. G. L. Frias and R. Nash, Microplastics: Finding a consensus on the definition, *Mar. Pollut. Bull.*, 2019, **138**, 145–147.

3 L. Hu, J. Fu, S. Wang, Y. Xiang and X. Pan, Microplastics generated under simulated fire scenarios: Characteristics, antimony leaching, and toxicity, *Environ. Pollut.*, 2021, **269**, 115905.

4 H. Liu and J. Yang, Magnetic polymeric ferric magnesium chloride: Fe species distribution, characterization and coagulation removal of microplastics in water, *New J. Chem.*, 2024, **48**, 12783–12792.

5 L. C. M. Lebreton and A. L. Andrady, Future scenarios of global plastic waste generation and disposal, *Palgrave Commun.*, 2019, **5**, 6.

6 S. Arossa, C. Martin, S. Rossbach and C. M. Duarte, Microplastic removal by Red Sea giant clam (Tridacna maxima), *Environ. Pollut.*, 2019, **252**, 1257–1266.

7 K. Hu, W. Tian, Y. Yang, G. Nie, P. Zhou, Y. Wang and S. Wang, Microplastics remediation in aqueous systems: Strategies and technologies, *Water Res.*, 2021, **198**, 117144.

8 L. Li, X. Zhong, M. Zheng, P. Wu, F. Yu, S. Ouyang and J. Ma, Adsorption/desorption behavior of degradable polylactic acid microplastics on bisphenol A under different aging conditions, *New J. Chem.*, 2024, **48**, 2594–2607.

9 S. Viswanathan, A. A. Pallikkara, F. Muhammed and A. Kallingal, Graphitic carbon nitride based fluorine-free hydrophobic sponges for the mitigation of microplastics, oil spillage, and harmful microbial growth in water, Mater, *Today Sustain*, 2024, **26**, 100751.

10 J. Piao, M. Lu, J. Ren, Y. Wang, T. Feng, Y. Wang and S. Kuang, MOF-derived LDH modified flame-retardant polyurethane sponge for high-performance oil-water separation: Interface engineering design based on bioinspiration, *J. Hazard. Mater.*, 2023, **444**, 130398.

11 Z. Wang, C. Sun, F. Li and L. Chen, Fatigue resistance, reusable and biodegradable sponge materials from plant protein with rapid water adsorption capacity for microplastics removal, *Chem. Eng. J.*, 2021, **415**, 129006.

12 W. Liu, J. Zhang, H. Liu, X. Guo, X. Zhang, X. Yao and T. Zhang, A review of the removal of microplastics in global wastewater treatment plants: Characteristics and mechanisms, *Environ. Int.*, 2021, **146**, 106277.

13 Y. Chen, T. Li, H. Hu, H. Ao, X. Xiong, H. Shi and C. Wu, Transport and fate of microplastics in constructed wetlands: a microcosm study, *J. Hazard. Mater.*, 2021, **415**, 125615.

14 H. Sadegh and G. A. M. Ali, Potential applications of nanomaterials in wastewater treatment: nanoadsorbents performance, *Adv. Treat. Tech. Ind. Wastewater*, IGI Global, 2019, pp. 51–61.

15 M. Haris, M. W. Khan, A. Zavabeti, N. Mahmood and N. Eshtiaghi, Self-assembly of C@FeO nanopillars on 2D-MOF for simultaneous removal of microplastic and dissolved contaminants from water, *Chem. Eng. J.*, 2023, **455**, 140390.

16 E. Tiwari, N. Singh, N. Khandelwal, F. A. Monikh and G. K. Darbha, Application of Zn/Al layered double hydroxides for the removal of nano-scale plastic debris from aqueous systems, *J. Hazard. Mater.*, 2020, **397**, 122769.

17 Y. Heo, E. H. Lee and S. W. Lee, Adsorptive removal of micron-sized polystyrene particles using magnetic iron oxide nanoparticles, *Chemosphere*, 2022, **307**, 135672L.S.O. Mota.

18 P. C. O. de Oliveira, B. S. Peixoto, E. S. Bezerra and M. C. de Moraes, Biochar applications in microplastic and nanoplastic removal: mechanisms and integrated approaches, *Environ. Sci.: Water Res. Technol.*, 2025, **11**, 222–241.

19 F. Pasanen, R. O. Fuller and F. Maya, Fast and simultaneous removal of microplastics and plastic-derived endocrine disruptors using a magnetic ZIF-8 nanocomposite, *Chem. Eng. J.*, 2023, **455**, 140405.

20 A. Zhu, J. Zheng, Z. Zhu, C. Hu and B. Liu, Enhanced superhydrophobic melamine sponge with bimetal organic framework for simultaneous oil–water separation and microplastic removal, *Colloids Surf., A*, 2024, **696**, 134295.

21 C. Qi, L. Zhao, Y. Lin and D. Wu, Graphene oxide/chitosan sponge as a novel filtering material for the removal of dye from water, *J. Colloid Interface Sci.*, 2018, **517**, 18–27.

22 H. Li, Q. P. Luo, S. Zhao, Y. Y. Zhou, F. Y. Huang, X. R. Yang and J. Q. Su, Effect of phenol formaldehyde-associated microplastics on soil microbial community, assembly, and functioning, *J. Hazard. Mater.*, 2023, **443**, 130288.

23 S. Barthwal, S. Barthwal, B. Singh and N. B. Singh, Multifunctional and fluorine-free superhydrophobic composite coating based on PDMS modified MWCNTs/ZnO with self-cleaning, oil–water separation, and flame retardant properties, *Colloids Surf., A*, 2020, **597**, 124776.

24 X. M. Dai, N. Sun, S. O. Nielsen, B. B. Stogin, J. Wang, S. K. Yang and T. S. Wong, Hydrophilic directional slippery rough surfaces for water harvesting, *Sci. Adv.*, 2018, **4**, eaaq0919.

25 V. Dichiarante, R. Milani and P. Metrangolo, Natural surfactants towards a more sustainable fluorine chemistry, *Green Chem.*, 2018, **20**, 13–27.

26 K. W. Huang and S. W. Kuo, High-performance polybenzoxazine nanocomposites containing multifunctional POSS cores presenting vinyl-terminated benzoxazine groups, *Macromol. Chem. Phys.*, 2010, **211**, 2301–2311.

27 N. Moradi, G. Soufi, A. Kabir, M. Karimi and H. Bagheri, Polyester fabric-based nano copper-polyhedral oligomeric silsesquioxanes sorbent for thin film extraction of non-steroidal anti-inflammatory drugs, *Anal. Chim. Acta*, 2023, **1270**, 341461.

28 P. Loganathan, K. K. R. Datta and S. Shanmugan, A superhydrophobic covalent zeolitic imidazolate framework–polyhedral oligomeric silsesquioxane hybrid material as a highly efficient and reusable sorbent for organic solvents, *Inorg. Chem. Front.*, 2021, **8**, 2288–2298.

29 P. Zhang, B. Qin and J. Xia, UV curable robust durable hydrophobic coating based on epoxy polyhedral oligomeric silsesquioxanes (EP-POSS) and their derivatives, *ACS Omega*, 2022, **7**, 17108–17118.

30 L. Hao, Y. Zhang, H. Liu, S. Wang, X. Li and Y. Chen, Preparation and study of highly hydrophobic and strongly oleophilic reticulated polyurethane foam surface modified with polydopamine and polyhedral oligomeric silsesquioxane, *J. Appl. Polym. Sci.*, 2025, e57125.

31 W. Li and H. Liu, Novel organic–inorganic hybrid polymer based on fluorinated polyhedral oligomeric silsesquioxanes for stable superamphiphobic fabrics and aluminum corrosion protection, *Mater. Today Chem.*, 2023, **29**, 101390.

32 H. Zhao, W. She, D. Shi, W. Wu, Q. C. Zhang and R. K. Li, Polyurethane/POSS nanocomposites for superior hydrophobicity and high ductility, *Composites, Part B*, 2019, **177**, 107441.

33 H. Lin, X. Wan, X. Jiang, Q. Wang and J. Yin, A ''thiol–ene'' photo-curable hybrid fluorinated resist for the high-performance replica mold of nanoimprint lithography (NIL), *J. Mater. Chem.*, 2012, **22**, 2616–2623.

34 P. Zhang, S. Xing, Z. Lin, Z. Zhao, H. Kong and J. Li, Thiol–ene click chemistry for constructing transition layer to enhance the interface interaction between polyacrylonitrile fiber and styrene–butadiene–styrene modified asphalt, *J. Appl. Polym. Sci.*, 2024, **141**, e55381.

35 S. Foorginezhad and M. Zerafat, Effect of solvent properties on crystallinity and morphology of octavinyl-POSS: a comparative study, *J. Nanostruct.*, 2020, **10**, 375–391.

36 D. Chen, J. Nie, S. Yi, W. Wu, Y. Zhong, J. Liao and C. Huang, Thermal behaviour and mechanical properties of novel RTV silicone rubbers using divinyl-hexa(trimethoxysilyl)ethyl-POSS as cross-linker, *Polym. Degrad. Stab.*, 2010, **95**, 618–626.

37 V. P. Dinh, H. M. Le, V. D. Nguyen, V. A. Dao, N. Q. Hung, L. A. Tuyen and L. V. Tan, Insight into the adsorption mechanisms of methylene blue and chromium(III) from aqueous solution onto pomelo fruit peel, *RSC Adv.*, 2019, **9**, 25847–25860.

38 M. Samanta, S. Roychowdhury and D. Mitra, Studies on sorption kinetics and sorption isotherm for pervaporative separation of benzene from model pyrolysis gasoline using in situ nano silver/polyvinyl alcohol membrane, *J. Environ. Sci. Health, Part A*, 2021, **56**, 1397–1408.

39 V. O. Shikuku and S. Jemutai-Kimosop, Efficient removal of sulfamethoxazole onto sugarcane bagasse-derived biochar: two and three-parameter isotherms, kinetics and thermodynamics, *S. Afr. J. Chem.*, 2020, **73**, 111–119.

40 R. Zhang, X. Jing, Y. Chu, L. Wang, W. Kang, D. Wei and S. Xiong, Nitrogen/oxygen co-doped monolithic carbon electrodes derived from melamine foam for high-performance supercapacitors, *J. Mater. Chem. A*, 2018, **6**, 17730–17739.

41 W. Zhang, X. Zhai, T. Xiang, M. Zhou, D. Zang, Z. Gao and C. Wang, Superhydrophobic melamine sponge with excellent surface selectivity and fire retardancy for oil absorption, *J. Mater. Sci.*, 2017, **52**, 73–85.

42 K. Xu, C. Wu, Z. Chen, M. Li, L. Yang, S. Ai and S. Cui, Preparation and characterization of lightweight, hydrophobic, and insulative melamine foam/fumed silica composites, *ACS Appl. Mater. Interfaces*, 2025, **17**, 12653–12662.

43 C. H. Xue, Q. Q. Fan, X. J. Guo, Q. F. An and S. T. Jia, Fabrication of superhydrophobic cotton fabrics by grafting of POSS-based polymers on fibers, *Appl. Surf. Sci.*, 2019, **465**, 241–248.

44 P. Dong, H. Liu, S. Xu, C. Chen, S. Feng and A. Long, Sheet-like skeleton carbon derived from shaddock peels with hierarchically porous structures for ultra-fast removal of methylene blue, *Water*, 2021, **13**, 2554.

45 S. Chatterjee, S. Sen Gupta and G. Kumaraswamy, Omniphilic polymeric sponges by ice templating, *Chem. Mater.*, 2016, **28**, 1823–1831.

46 S. S. Gupta and K. G. Bhattacharyya, Kinetics of adsorption of metal ions on inorganic materials: a review, *Adv. Colloid Interface Sci.*, 2011, **162**, 39–58.

47 F. Zhang, X. Tang, Y. Huang, A. A. Keller and J. Lan, Competitive removal of Pb^{2+} and malachite green from water by magnetic phosphate nanocomposites, *Water Res.*, 2019, **150**, 442–451.

48 N. A. Oladoja, A critical review of the applicability of Avrami fractional kinetic equation in adsorption-based water treatment studies, *Desalin. Water Treat.*, 2016, **57**(34), 15813–15825.

49 M. Bhaumik, S. Agarwal, V. K. Gupta and A. Maity, Enhanced removal of Cr(VI) from aqueous solutions using polypyrrole wrapped oxidized MWCNTs nanocomposite adsorbent, *J. Colloid Interface Sci.*, 2016, **470**, 257–267.

50 L. Wang, J. Zhang, R. Zhao, C. Li, Y. Li and C. Zhang, Adsorption of basic dyes on activated carbon prepared from *Polygonum orientale* Linn: equilibrium, kinetic and thermodynamic studies, *Desalination*, 2010, **254**, 68–74.

51 Z. Wu, H. Zhong, X. Yuan, H. Wang, L. Wang, X. Chen, G. Zeng and Y. Wu, Adsorptive removal of methylene blue by rhamnolipid-functionalized graphene oxide from wastewater, *Water Res.*, 2014, **67**, 330–344.

52 S. Zafar, M. I. Khan, M. Khraisheh, S. Shahida, T. Javed, M. L. Mirza and N. Khalid, Use of rice husk as an effective sorbent for the removal of cerium ions from aqueous solution: kinetic, equilibrium and thermodynamic studies, *Desalin. Water Treat.*, 2019, **150**, 124–135.

53 K. I. Andersson, M. Eriksson and M. Norgren, Removal of lignin from wastewater generated by mechanical pulping using activated carbon and fly ash: adsorption isotherms and thermodynamics, *Ind. Eng. Chem. Res.*, 2011, **50**, 7722–7732.

54 Z. Aksu and Ö. Tunç, Application of biosorption for penicillin G removal: comparison with activated carbon, *Process Biochem.*, 2005, **40**, 831–847.

55 P. S. Tourinho, V. Kočí, S. Loureiro and C. A. M. van Gestel, Partitioning of chemical contaminants to microplastics: sorption mechanisms, environmental distribution and effects on toxicity and bioaccumulation, *Environ. Pollut.*, 2019, **252**, 1246–1256.

56 B. Shang, Y. Wang, B. Peng and Z. Deng, Bioinspired polydopamine particles-assisted construction of superhydrophobic surfaces for oil/water separation, *J. Colloid Interface Sci.*, 2016, **482**, 240–251.

57 Y. Liu, J. Ma, T. Wu, X. Wang, G. Huang, Y. Liu and J. Gao, Cost-effective reduced graphene oxide-coated polyurethane sponge as a highly efficient and reusable oil-absorbent, *ACS Appl. Mater. Interfaces*, 2013, **5**, 10018–10026.

58 C. Sun, Z. Wang, L. Chen and F. Li, Fabrication of robust and compressive chitin and graphene oxide sponges for removal of microplastics with different functional groups, *Chem. Eng. J.*, 2020, **393**, 124796.

59 M. Ko, T. Jang, S. Yoon, J. Lee, J. H. Choi, J. W. Choi and J. A. Park, Synthesis of recyclable and light-weight graphene oxide/chitosan/genipin sponges for the adsorption of diclofenac, triclosan, and microplastics, *Chemosphere*, 2024, **356**, 141956.

60 H. Li, M. Tang, J. Wang, L. Dong, L. Wang, Q. Liu and S. Lu, Theoretical and experimental investigation on rapid and efficient adsorption characteristics of microplastics by magnetic sponge carbon, *Sci. Total Environ.*, 2023, **897**, 165404.

61 R. Ma, Y. Feng, J. Yu, X. Zhao, Y. Du and X. Zhang, Ultralight sponge made from sodium alginate with processability and stability for efficient removal of microplastics, *Environ. Sci. Pollut. Res.*, 2023, **30**, 104135–104147.

62 A. Uheida, H. G. Mejía, M. Abdel-Rehim, W. Hamd and J. Dutta, Visible light photocatalytic degradation of polypropylene microplastics in a continuous water flow system, *J. Hazard. Mater.*, 2021, **406**, 124299.

63 T. T. V. Ha, N. M. Viet, P. T. Thanh and V. T. Quan, Loofah plant-derived biodegradable superhydrophobic sponge for

effective removal of oil and microplastic from water, *Environ. Technol. Innovation*, 2023, **32**, 103265.
64 Z. Zhu, X. Wu and Z. Wang, Effect of polyaniline dispersibility in chitin sponge matrix controlled by hydrophilicity on microplastics adsorption, *Int. J. Biol. Macromol.*, 2023, **253**, 127292.
65 J. Fu, N. Liu, Y. Peng, G. Wang, X. Wang, Q. Wang and L. Chen, An ultra-light sustainable sponge for elimination of microplastics and nanoplastics, *J. Hazard. Mater.*, 2023, **456**, 131685.
66 O. Duman, U. Cengiz, C. Ö. Diker, S. M. Güreşir, S. Tunc and C. Cengiz, Fabrication of superhydrophobic sorbent material via in situ coating of melamine sponge with halloysite nanotube and fluoroalkylsilane using supercritical CO_2 coating system for efficient oily water treatment, *Sep. Purif. Technol.*, 2025, **360**, 131069.
67 A. B. Olabintan and T. A. Saleh, Sequestration of oils from water using superhydrophobic silanized montmorillonite-KSF nanoclay coated polyurethane foam, *React. Funct. Polym.*, 2024, **195**, 105807.
68 O. Duman, U. Cengiz, C. Ö. Diker, C. Cengiz, S. M. Güreşir and S. Tunc, Fabrication of superhydrophobic melamine sponge composite sorbent in supercritical carbon dioxide atmosphere for selective and effective oil removal from water, *J. Environ. Chem. Eng.*, 2023, **11**, 111602.
69 H. Wang, E. Wang, Z. Liu, D. Gao, R. Yuan, L. Sun and Y. Zhu, A novel carbon nanotubes reinforced superhydrophobic and superoleophilic polyurethane sponge for selective oil–water separation through a chemical fabrication, *J. Mater. Chem. A*, 2015, **3**, 266–273.
70 C. Su, H. Yang, H. Zhao, Y. Liu and R. Chen, Recyclable and biodegradable superhydrophobic and superoleophilic chitosan sponge for the effective removal of oily pollutants from water, *Chem. Eng. J.*, 2017, **330**, 423–432.
71 O. Duman, C. Cengiz, C. Ö. Diker, U. Cengiz, S. M. Güreşir and S. Tunç, Development of a superhydrophobic and superoleophilic halloysite nanotube/phenyltriethoxysilane-coated melamine sponge sorbent material with high performance in supercritical CO_2 atmosphere for the selective and effective oil spill cleanup and oil–water separation, *J. Environ. Manage.*, 2025, **373**, 123715.
72 H. Wang, Q. Zhao, K. Zhang, F. Wang, J. Zhi and C.-X. Shan, Superhydrophobic-functionalized melamine sponge for oil/water separation, *Langmuir*, 2022, **38**, 11304–11313.
73 L. He, X. Zhang, Y. Zhao, J. Liu, F. Wang and Q. Li, Superhydrophobic sponge with self-cleaning properties for continuous and efficient oil–water separation in harsh environment, *Constr. Build. Mater.*, 2024, **441**, 137505.
74 O. Duman, C. Cengiz, C. Ö. Diker, U. Cengiz, S. M. Güreşir and S. Tunc, Effect of alkoxysilane chain length on the surface, stability, sorption and oil–water separation properties of novel superhydrophobic porous sorbent materials produced using innovative drainage technique in $scCO_2$ atmosphere, *Sep. Purif. Technol.*, 2024, **345**, 127354.
75 Y. Zhang, N. Zhang, S. Zhou, X. Lv, C. Yang, W. Chen and W. Jiang, Facile preparation of ZIF-67 coated melamine sponge for efficient oil/water separation, *Ind. Eng. Chem. Res.*, 2019, **58**, 17380–17388.
76 Y. Yang, Y. Deng, Z. Tong and C. Wang, Multifunctional foams derived from poly (melamine formaldehyde) as recyclable oil absorbents, *J. Mater. Chem. A*, 2014, **2**, 9994–9999.
77 X. Dong, M. Cui, R. Huang, R. Su, W. Qi and Z. He, Polydopamine-assisted surface coating of MIL-53 and dodecanethiol on a melamine sponge for oil–water separation, *Langmuir*, 2020, **36**, 1212–1220.
78 X. Han, J. Hu, K. Chen, P. Wang, G. Zhang, J. Gu and F. Cao, Self-assembly and epitaxial growth of multifunctional micro-nano-spheres for effective separation of water-in-oil emulsions with ultra-high flux, *Chem. Eng. J.*, 2018, **352**, 530–538.
79 J. Chen, X. Zhang, L. Zhang, X. Jiang, F. Xiao, J. Hu and J. Ding, Directional self-assembly of octavinyl polyhedral oligomeric silsesquioxane on the surface of melamine sponge: establishing hydrophobic surfaces to improve oil–water separation performance, *J. Mol. Liq.*, 2024, **404**, 124941.
80 M. Li, Y. Fang, C. Liu, M. Zhou, X. Miao, Y. Pei and L. Wu, Facile generation of highly durable thiol-functionalized polyhedral oligomeric silsesquioxane based superhydrophobic melamine foam, *Front. Chem. Sci. Eng.*, 2022, **16**, 1247–1258.
81 K. Dharmaraj, M. S. Kumar, N. Palanisami, M. Prakash, P. Loganathan and S. Shanmugan, Eco-friendly porous composite of octaphenyl polyhedral oligomeric silsesquioxane and HKUST-1 with hydrophobic–oleophilic properties towards sorption of oils and organic solvents, *Dalton Trans.*, 2024, **53**, 13602–13616.
82 P. Loganathan, R. Yogapriya, A. Chinnusamy, K. K. R. Datta and S. Shanmugan, In situ growth of octa-phenyl polyhedral oligomeric silsesquioxane nanocages over fluorinated graphene nanosheets: super-wetting coatings for oil and organic sorption, *Dalton Trans.*, 2025, **54**, 1150–1163.